Electronic Supplementary Material (ESI) for Journal of Materials Chemistry A.

Supplementary Information

Transition metal single atom embedded GaN monolayer surface for efficient and selective CO_2 electroreduction

Muhammad Umer‡ , Sohaib Umer‡, Rohit Anand, Jinhong Mun, Mohammad Zafari, Geunsik Lee* and Kwang S. Kim*

Center for Superfunctional Materials, Department of Chemistry, Ulsan National Institute of Science and Technology (UNIST), 50 UNIST-gil, Ulsan 44919, South Korea

* Corresponding authors: *E-mail: gslee@unist.ac.kr (G.L.), kimks@unist.ac.kr (K.S.K.)

‡ These authors contributed equally

Contents

Supplementary Figures

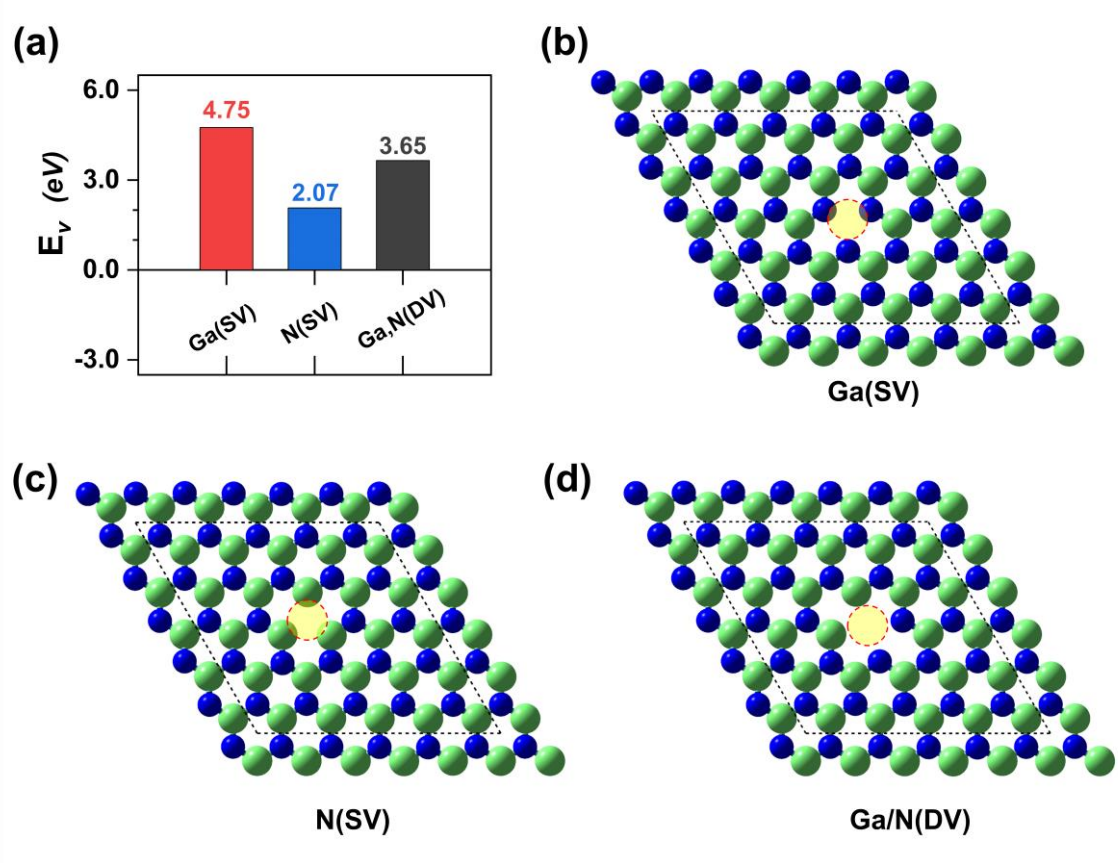

Fig. S1. (a) Vacancy formation energies ($E_{\mathrm{v}} = E_{\mathrm{d}} + \mu_{\mathrm{Ga/N}} - E_{\mathrm{prist}}$) of (b) Ga single vacancy (Ga-SV), (c) nitrogen single vacancy (N-SV), and (d) gallium-nitrogen double vacancy (Ga/N-DV) defect sites over GaN monolayer surface (Color code: Ga, light green; N, blue). Where $\mu_{\mathrm{Ga/N}}$ represents the chemical potential of Ga and N respectively, calculated with respect to bulk Ga and gaseous N_2, while the E_{prist} denotes the energy of pristine surface without any surface defect.

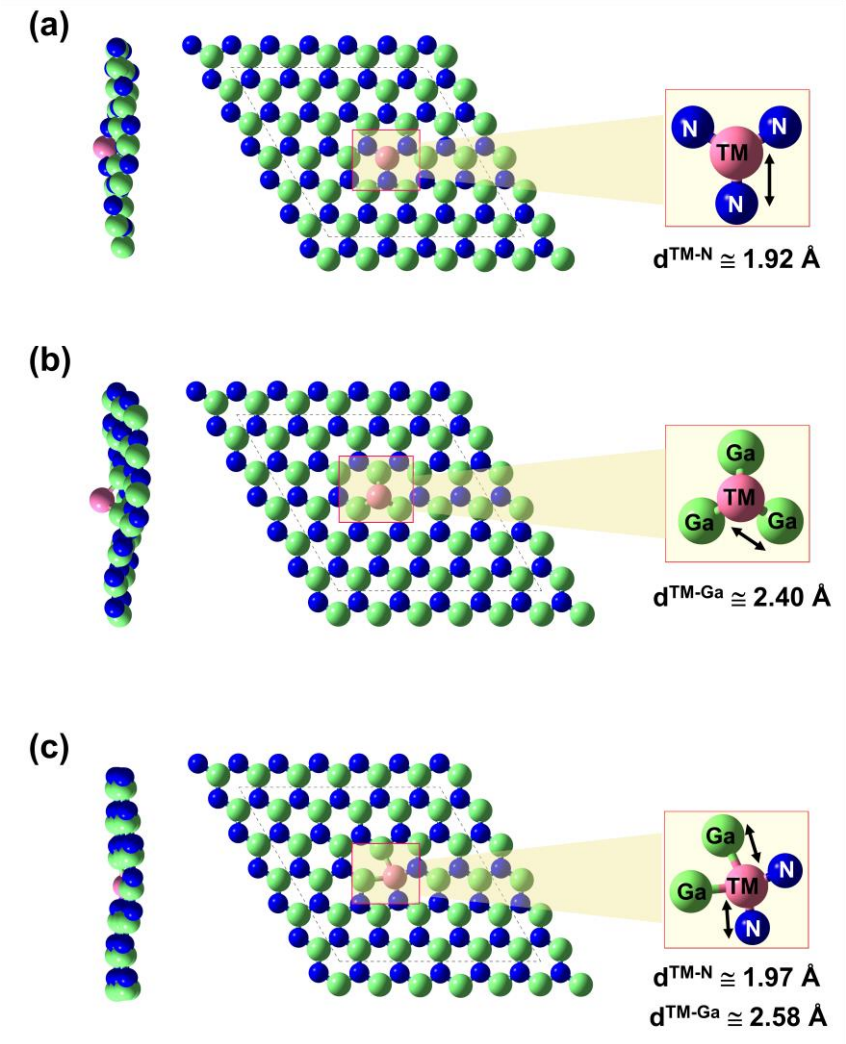

Fig. S2. Top and side views of (TM)SA embedded into (a) Ga-SV, (b) N-SV, and (c) Ga/N-DV defect sites. The distance from TM to nearest neighbor ($d^{TM-Ga/N}$) surface coordinating atoms are highlighted for each defect site of TM-SAC. Here the case for TM atom is Os (light pink).

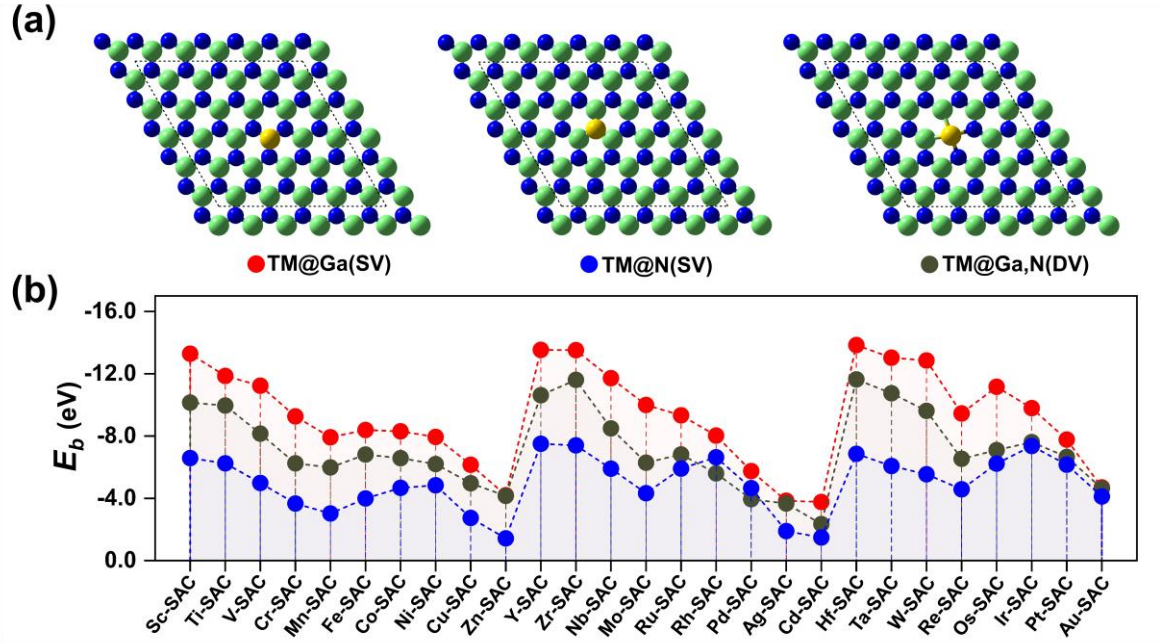

Fig. S3. (a) Geometric structures of (TM)SAs embedded into various defect sites including Ga-SV, N-SV, and Ga/N-DV sites. (b) TM binding energies (E_b) for each defect type surface. The more negative E_b values indicate the stronger metal-support interactions. Among the investigated defect type surfaces, TM-SAC(Ga-SV) structures showed a superior stability. (Color code: transition metal, golden; Ga, light green; N, blue).

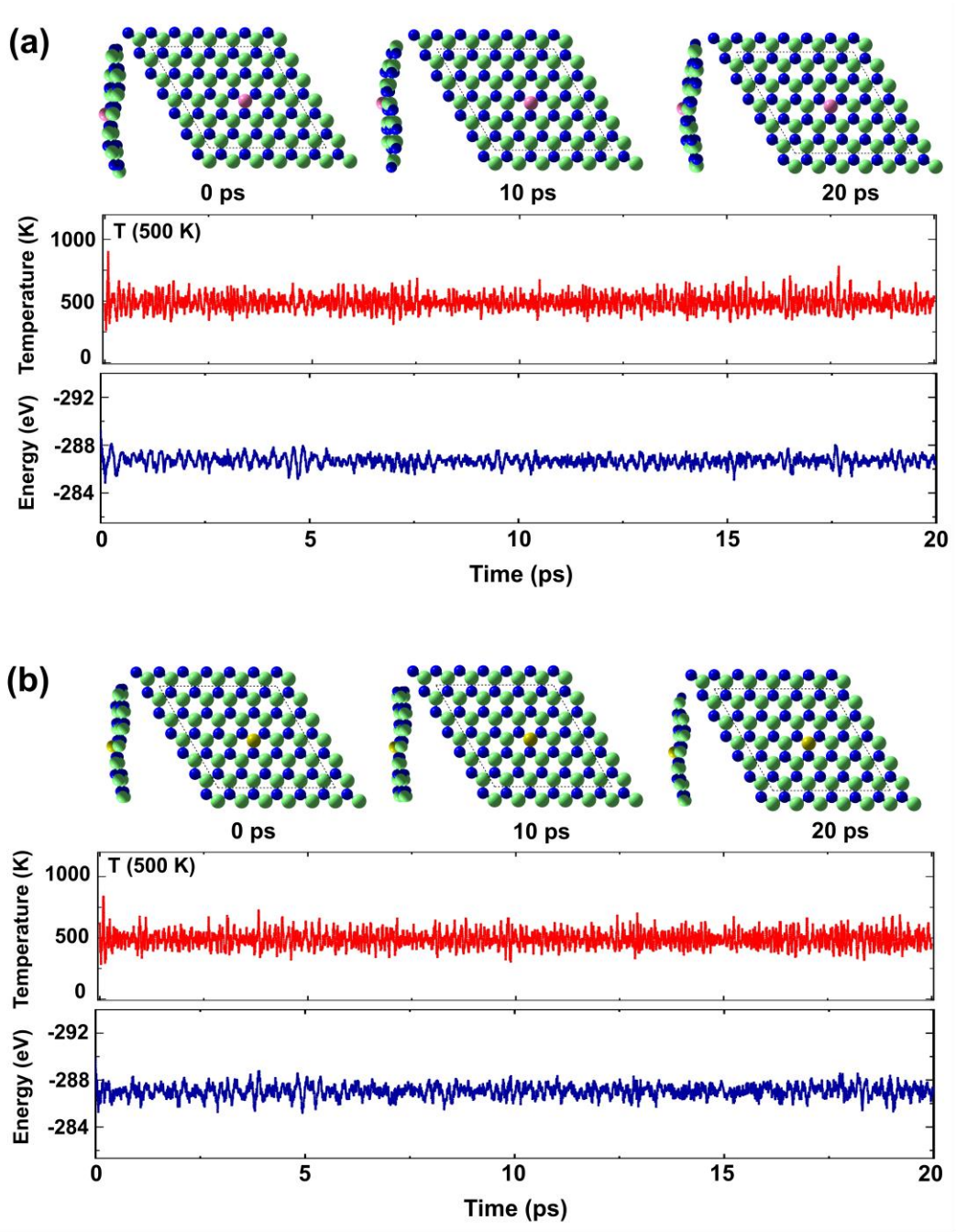

Fig. S4. Snapshots of the *ab initio* molecular dynamics simulation and corresponding energy and temperature profiles for (a) Os-SAC and (b) Ir-SAC, respectively. The temperature is controlled at 500 K whereas the small fluctuations in energy and temperature profile showing the representative structures are dynamically stable. (Color code: Os, light pink; Ir, golden-brown; Ga, light green; N, blue).

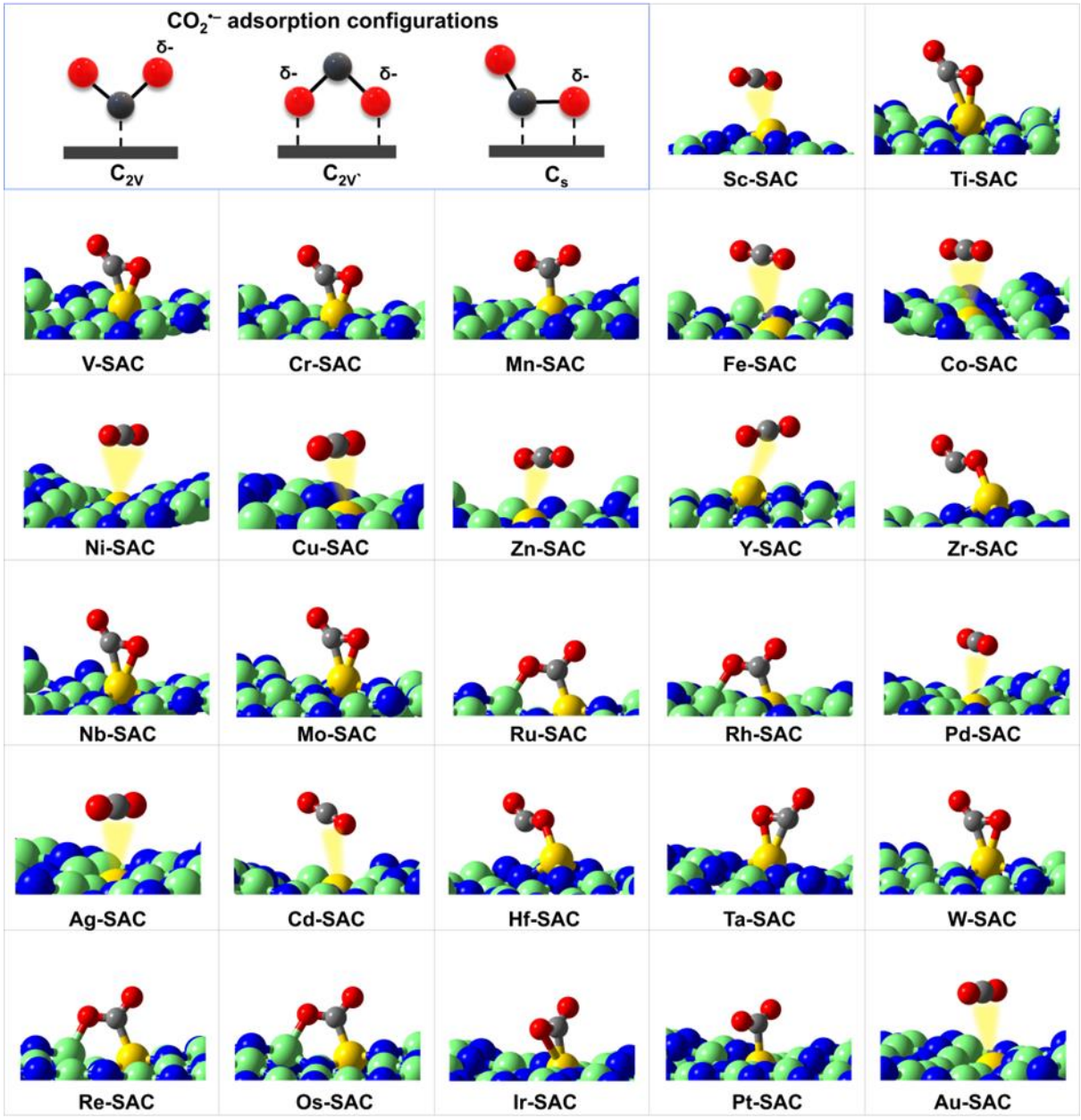

Fig. S5. Schematic illustration of possible CO_2 adsorption configurations and optimized CO_2 adsorbed geometries of all the considered systems. The golden filled line represents the physisorbed systems. The chemisorbed systems exhibit different types of CO_2 adsorption configurations either by sharing single metal active site in the mono- and bi-dentate fashion or the surface Ga atom stabilized configuration through Ga-O coordination (e.g Ru, Rh, Re and Os-SACs). (Color code: transition metal, golden; Ga, light green; N, blue; C, gray; O, red).

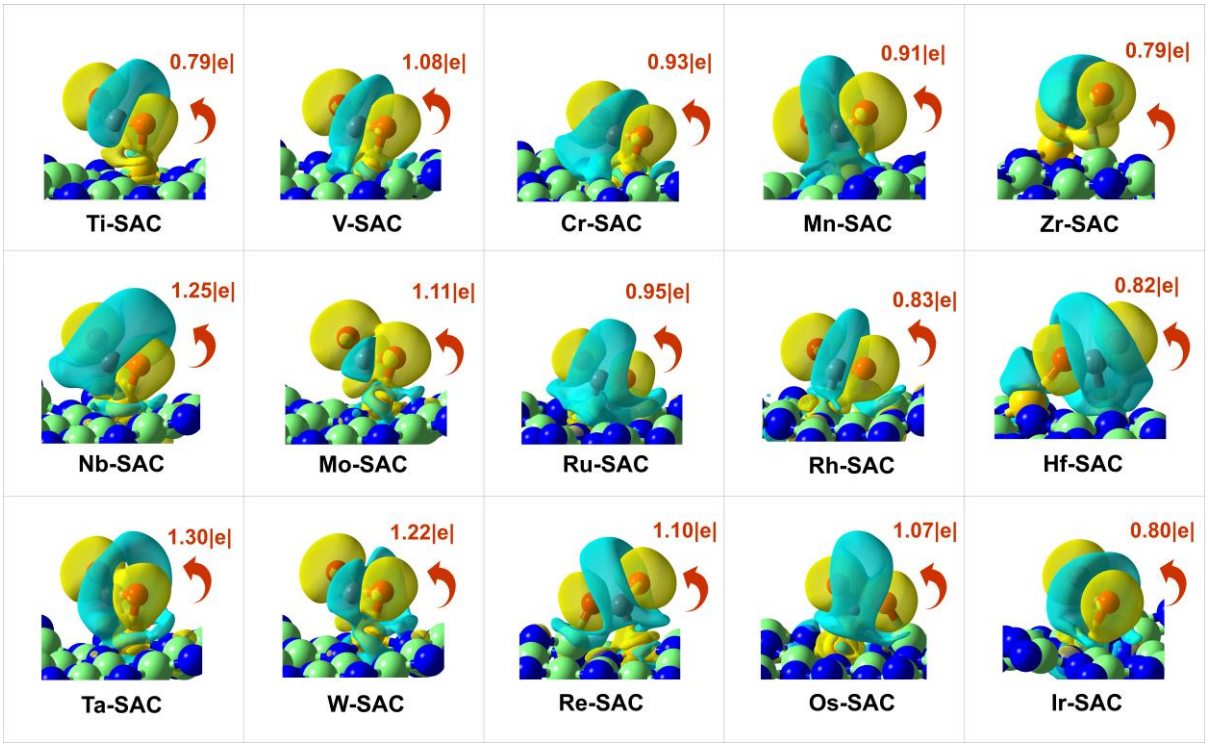

Fig. S6. The charge density difference plots of CO_2 chemisorbed over various TM-SACs showing a significant amount of charge transfer takes place from the surface to adsorbed CO_2 molecule. The isosurface value is 0.001563 e/Å^3. The charge depletion and accumulation are represented by cyan and yellow colors, respectively. The values given in red color indicate net Bader charge on $CO_2^{\bullet-}$ species.

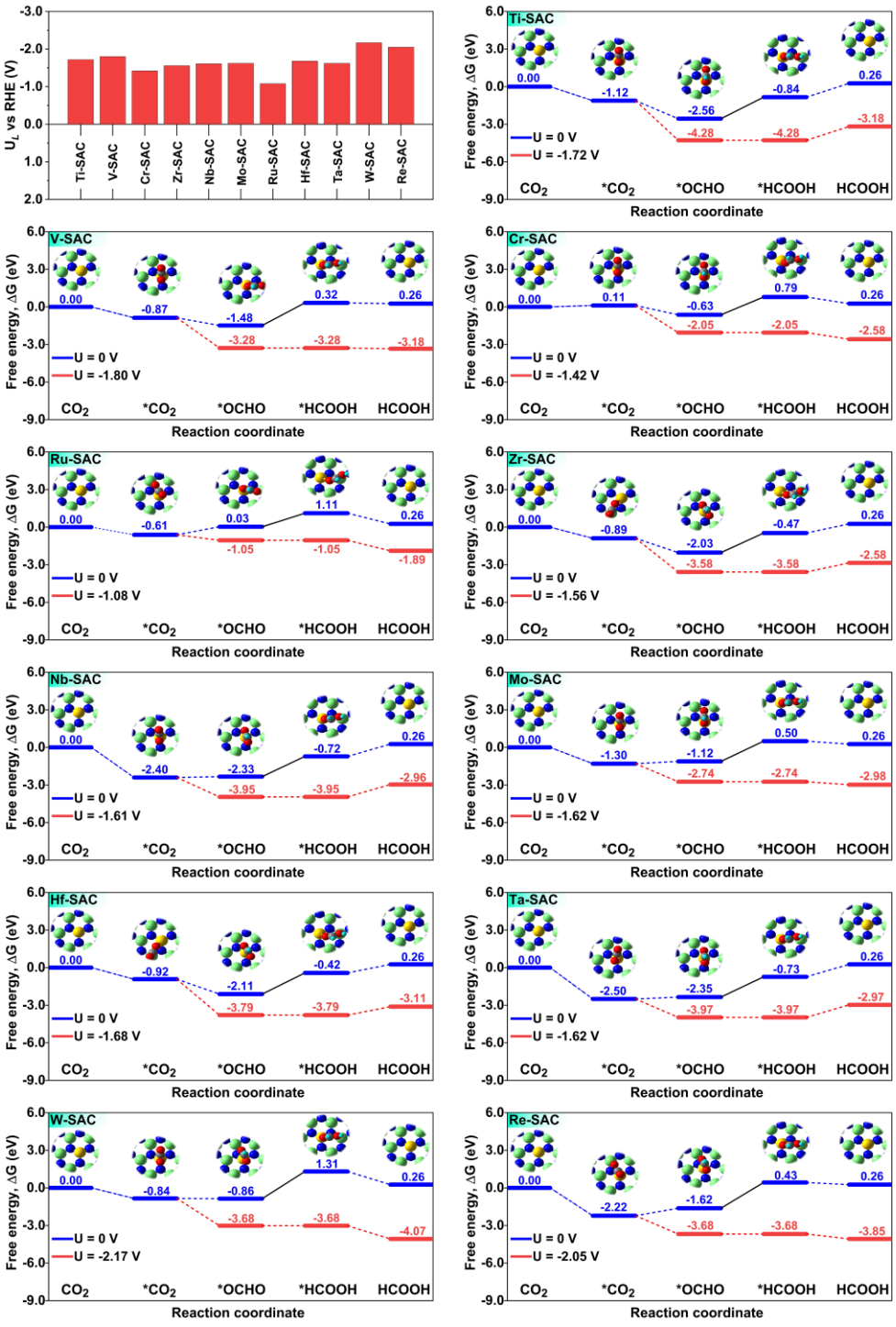

Fig. S7. Limiting potentials (U_L(s)) of Ti/V/Cr/Mn/Zr/Nb/Mo/Ru/Rh/Hf/Ta/W and Re embedded SACs for HCOOH formation. Free energy profiles for CO_2 reduction to HCOOH over different TM-SACs at zero and applied potential. The solid black line represents the potential-limiting step (PLS) of the catalytic pathway for HCOOH formation (Color code: transition metal, golden; Ga, light green; N, blue; C, gray; O, red; H, cyan).

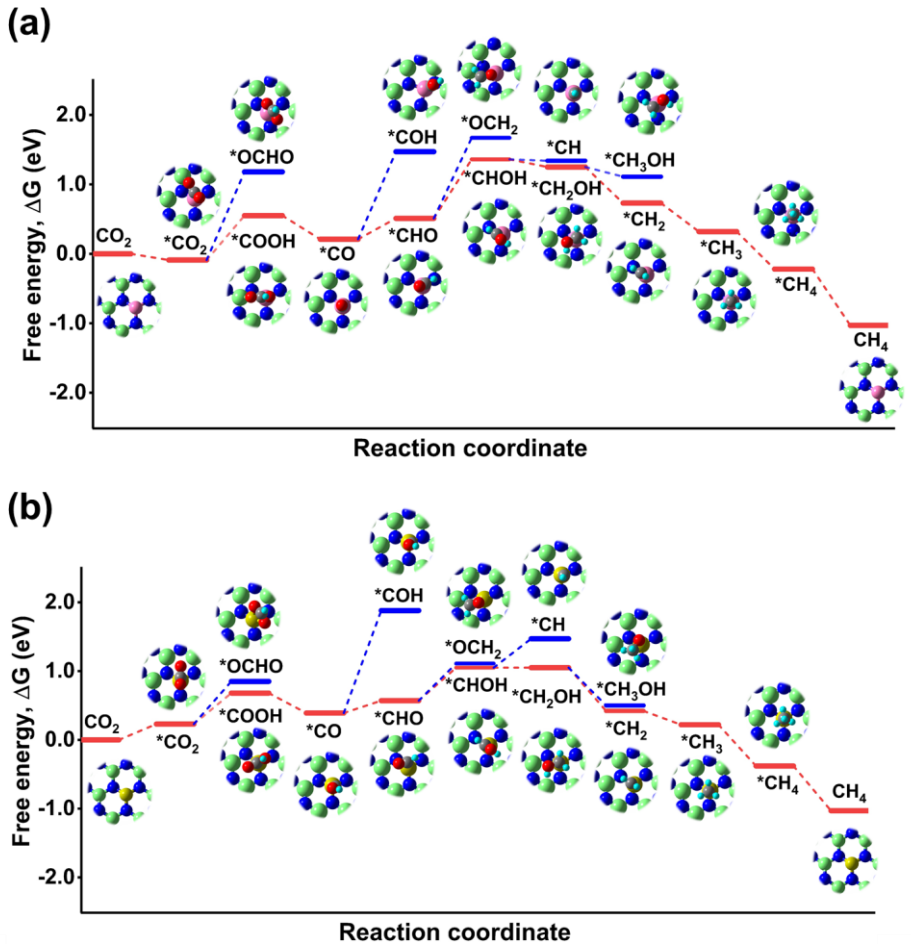

Fig. S8. Free energy diagrams for CO_2 reduction on (a) Os-SAC and (b) Ir-SAC along different pathways. The red and blue lines represent the energetically favorable and non-favorable pathways, respectively. (Color code: Os, light pink; Ir, golden-brown; Ga, light green; N, blue; C, gray; O, red; H, cyan).

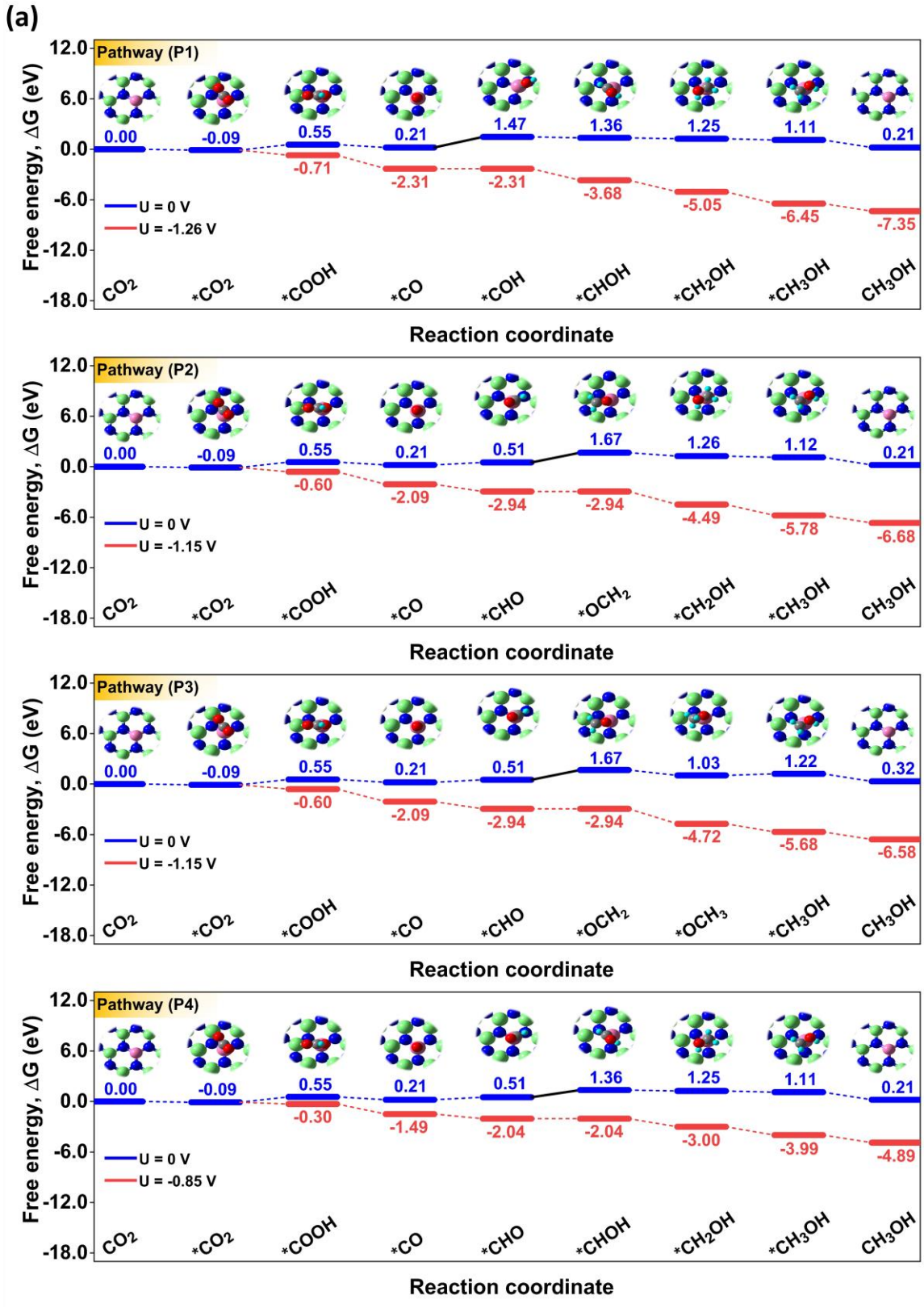

Fig. S9. (a) Free energy profiles of CO_2 reduction to CH_3OH on Os-SAC at zero and applied potential via different reduction pathways (P1 through P4). Solid black lines indicate the potential-limiting step (PLS) of the corresponding pathway. (Color code: Os, light pink; Ga, light green; N, blue; C, gray; O, red; H, cyan).

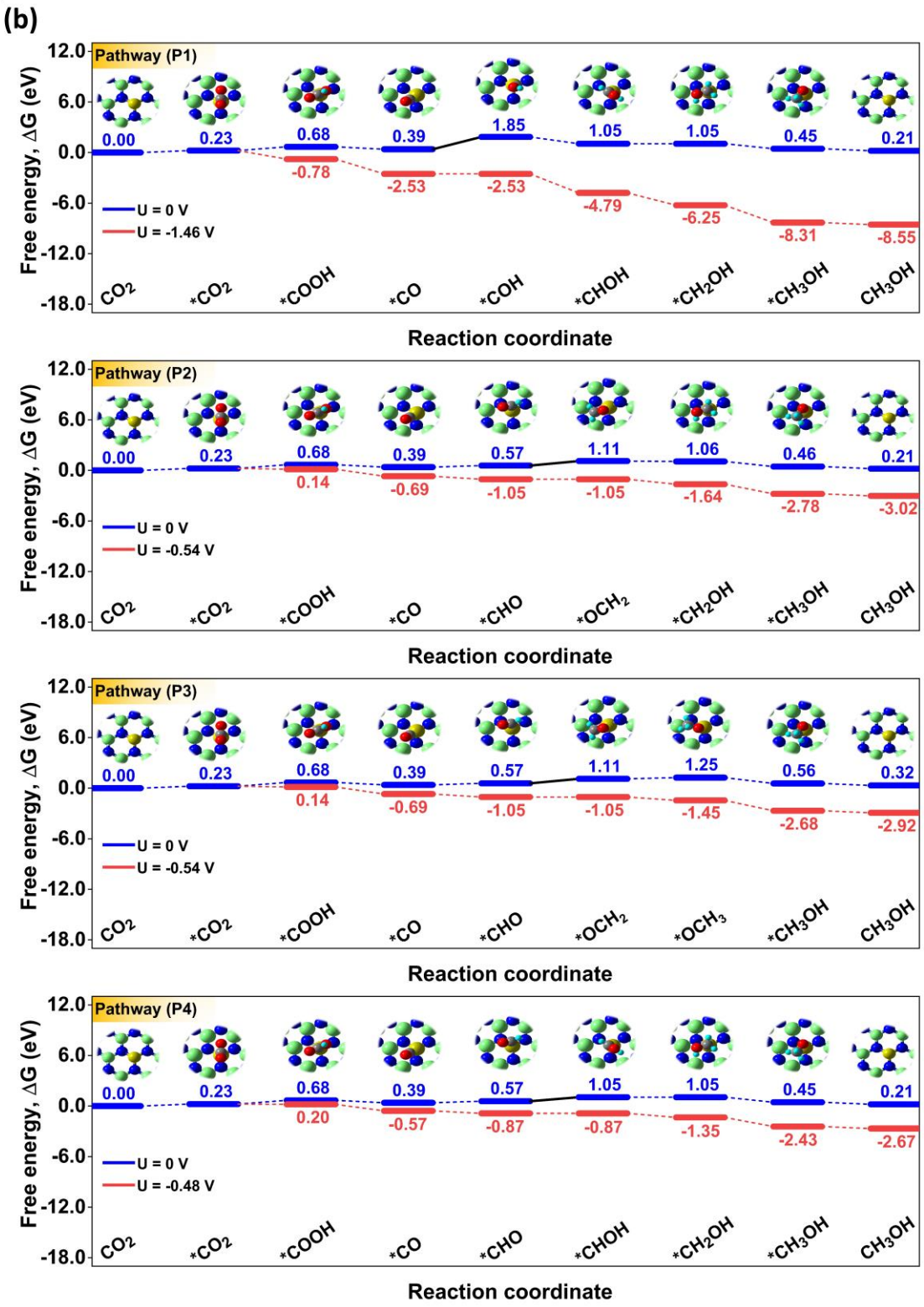

Fig. S9. (b) Free energy profiles of CO_2 reduction to CH_3OH over Ir-SAC at zero and applied potential via different reduction pathways (P1 through P4). Solid black lines indicate the potential-limiting step (PLS) of the corresponding pathway. (Color code: Ir, golden-brown; Ga, light green; N, blue; C, gray; O, red; H, cyan).

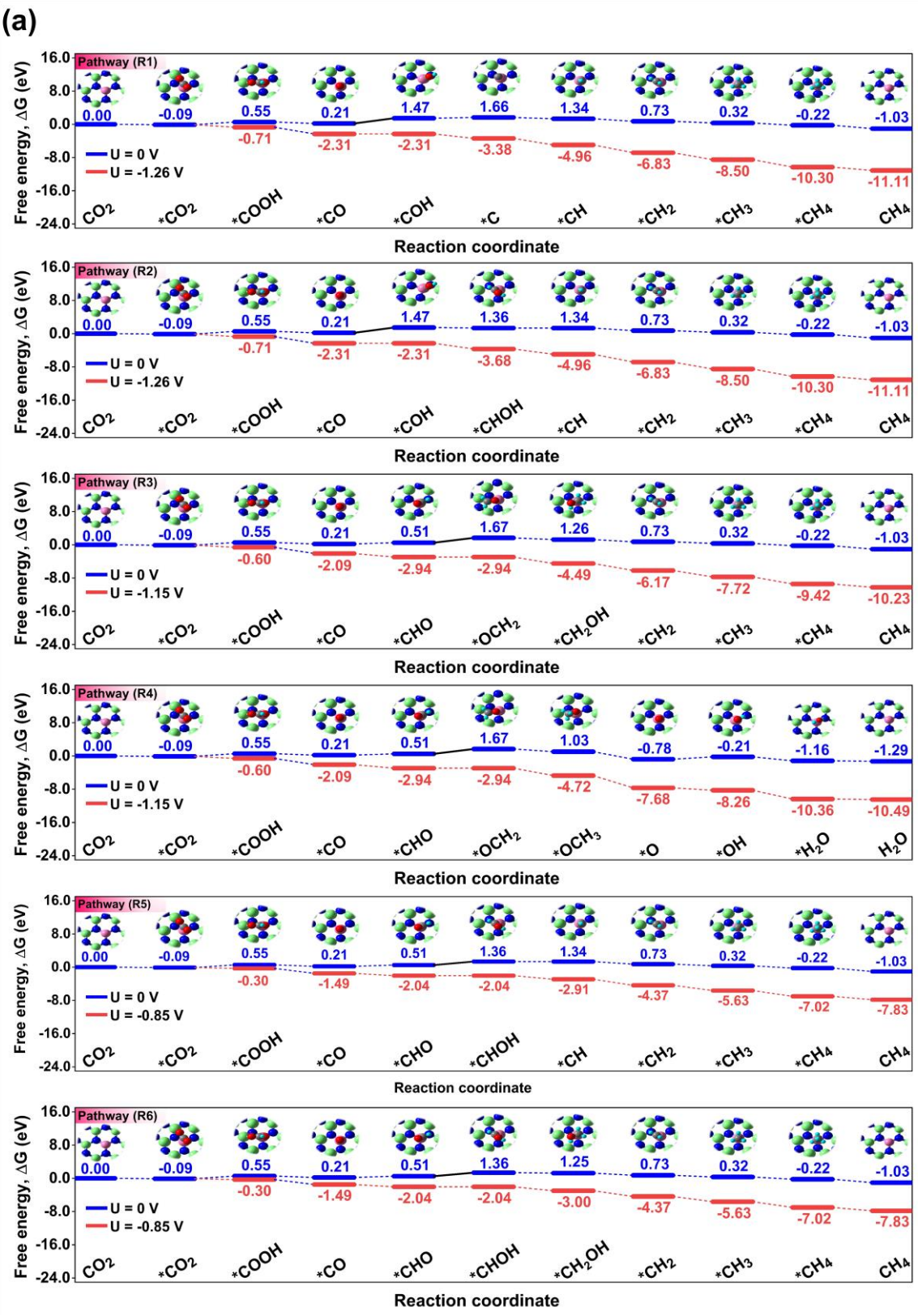

Fig. S10. (a) Free energy profiles of CO_2 reduction to CH_4 on Os-SAC at zero and applied potential via different reduction pathways (R1 through R6). Solid black lines indicate the potential-limiting step (PLS) of the corresponding pathway. (Color code: Os, light pink; Ga, light green; N, blue; C, gray; O, red; H, cyan).

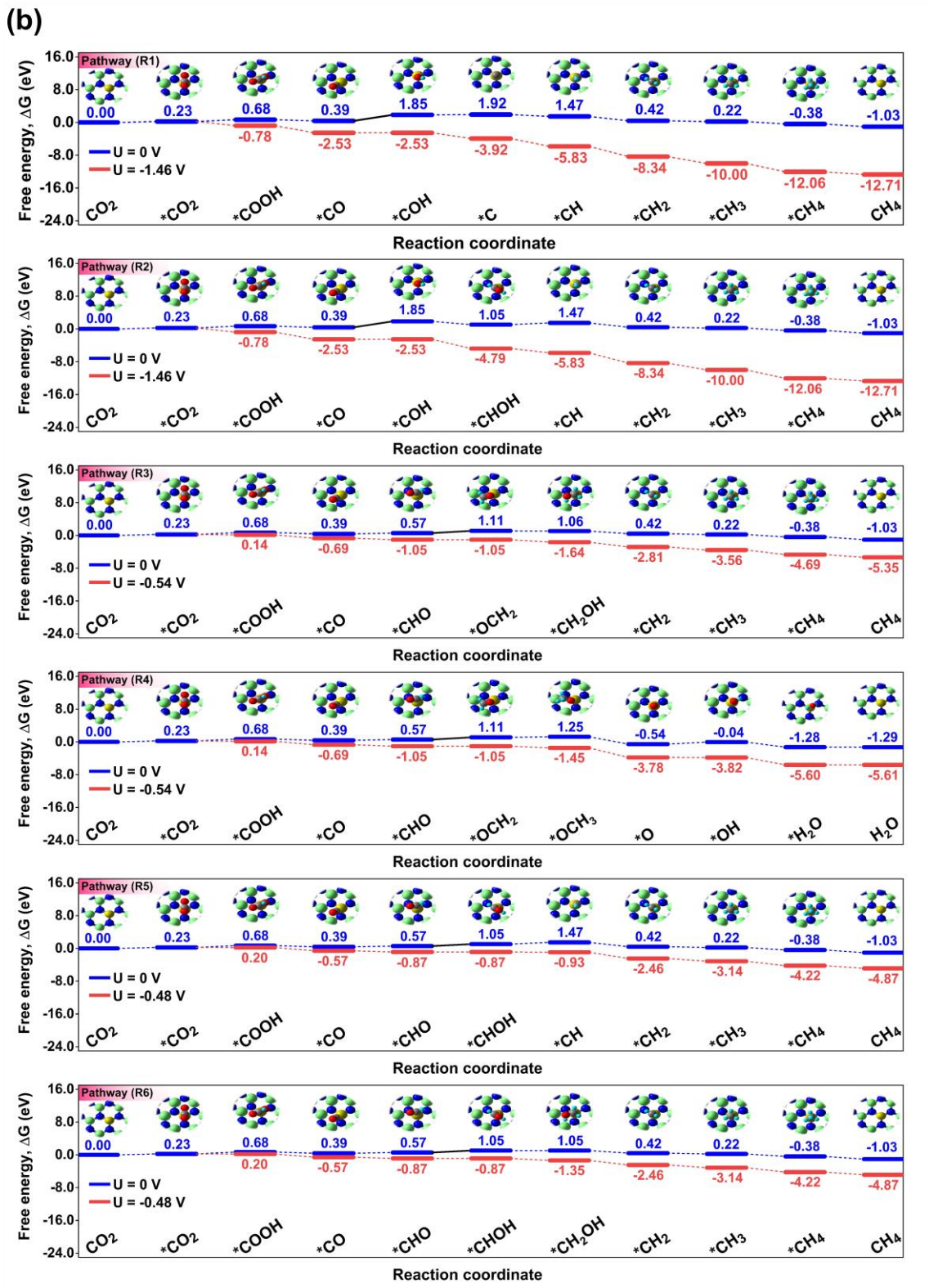

Fig. S10. (b) Free energy profiles of CO_2 reduction to CH_4 on Ir-SAC at zero and applied potential via different reduction pathways (R1 through R6). Solid black lines indicate the potential-limiting step (PLS) of the corresponding pathway. (Color code: Ir, golden-brown; Ga, light green; N, blue; C, gray; O, red; H, cyan).

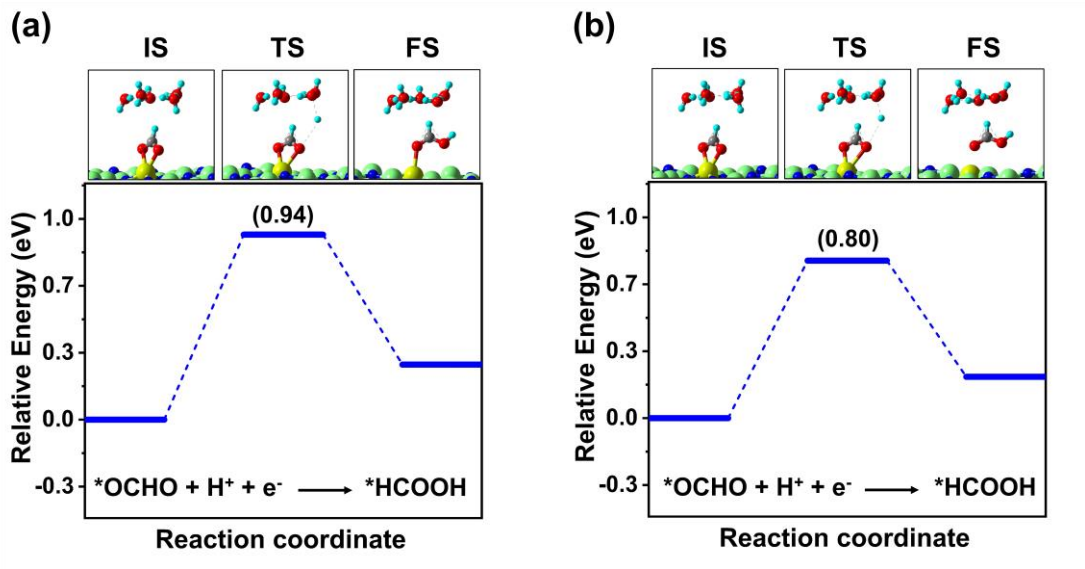

Fig. S11. Calculated kinetic energy barriers at the potential limiting steps for CO_2 reduction to HCOOH over (a) Mn- and (b) Rh-SACs. The (IS) initial state, (TS) transition state and (FS) final state are shown on top of the figure.

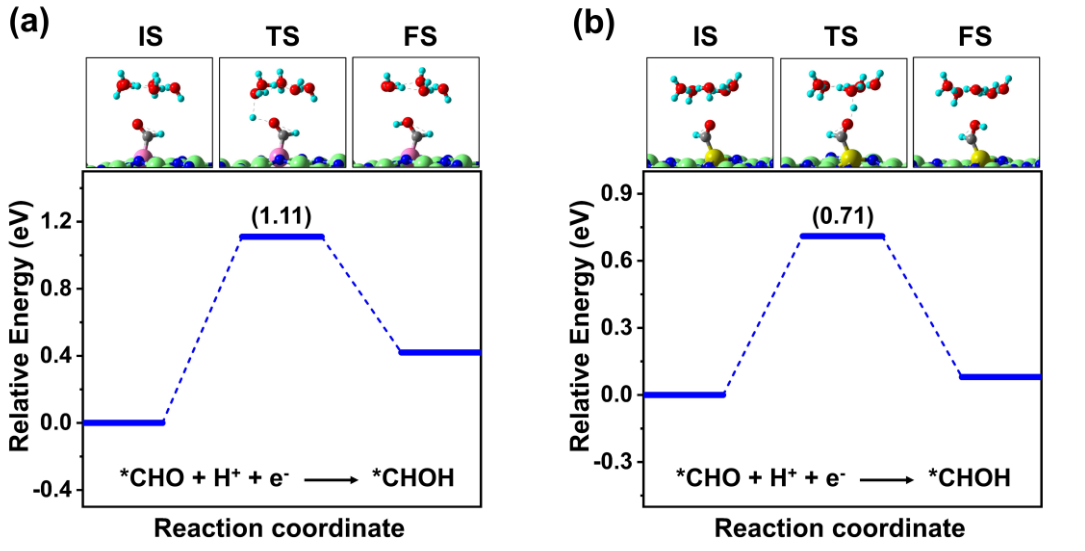

Fig. S12. Calculated kinetic energy barriers at the potential limiting steps for CO_2 reduction to CH_4 following the pathway R6 over (a) Os- and (b) Ir-SACs. The (IS) initial state, (TS) transition state and (FS) final state are shown on top of the figure.

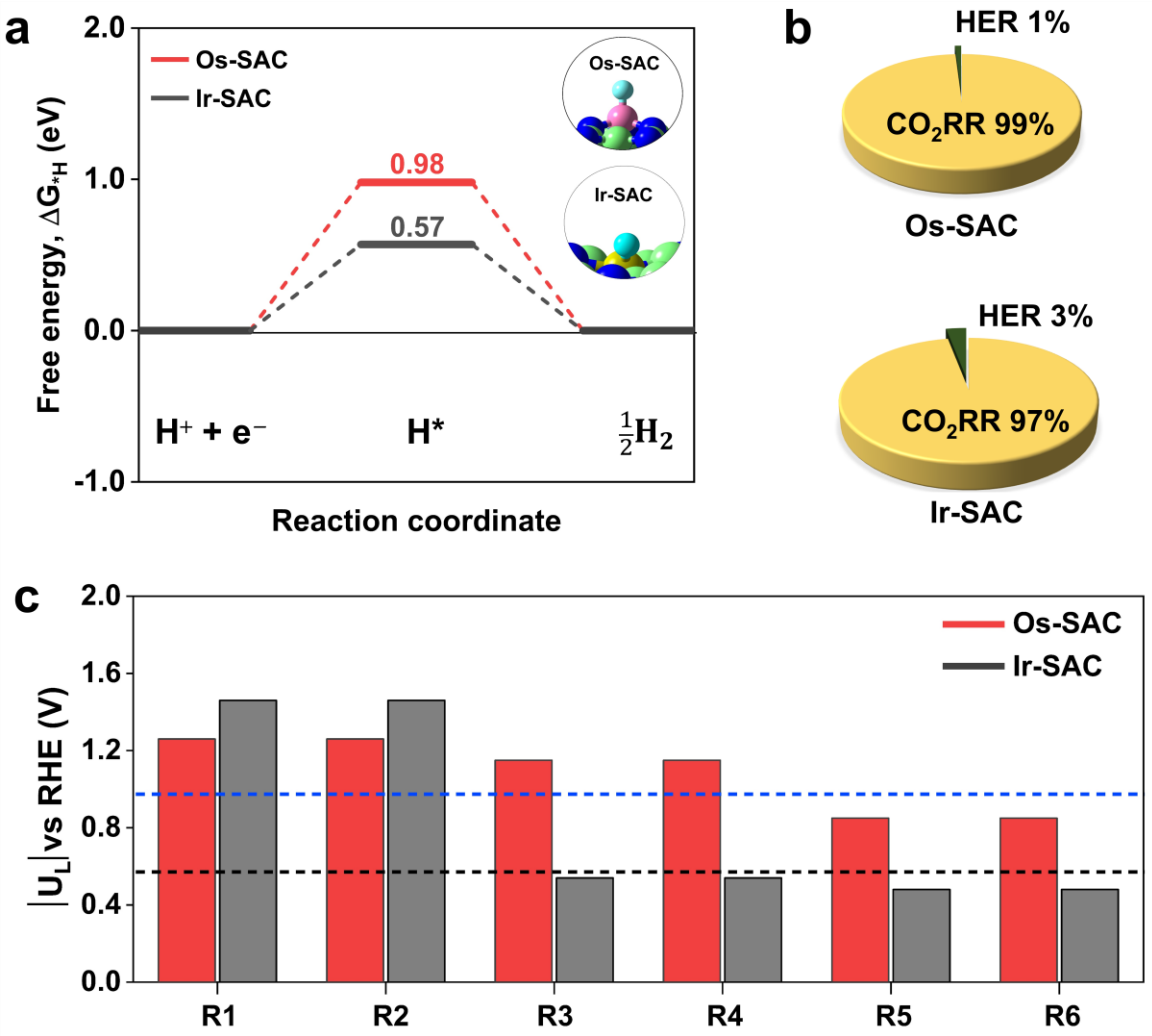

Fig. S13. (a) Free energy diagram of HER. The inset shows the H-adsorbed optimized geometries of Os-SAC and Ir-SAC (b) Faradaic efficiencies of the catalysts for CO_2RR with respect to its competitive HER and (c) U_L(s) of all the pathways considered in this study for CH_4 production, where blue and black dashed lines represent the U_L of HER for Os-SAC and Ir-SAC, respectively.

Supplementary Tables

Table S1. TM binding energies (E_b) for GaN monolayer surface. The E_b is provided for three different defect types, including Ga single vacancy (Ga-SV), Nitrogen single vacancy (N-SV), and gallium-nitrogen double vacancy (Ga/N-DV) sites.

Catalysts	E_b (eV)		
	Ga-SV	N-SV	Ga/N-DV
Sc-SAC	-13.29	-6.58	-10.15
Ti-SAC	-11.86	-6.25	-9.96
V-SAC	-11.23	-4.98	-8.15
Cr-SAC	-9.26	-3.67	-6.25
Mn-SAC	-7.92	-3.03	-5.99
Fe-SAC	-8.39	-3.99	-6.81
Co-SAC	-8.30	-4.67	-6.58
Ni-SAC	-7.94	-4.84	-6.20
Cu-SAC	-6.16	-2.74	-4.97
Zn-SAC	-4.20	-1.43	-4.16
Y-SAC	-13.54	-7.50	-10.62
Zr-SAC	-13.51	-7.40	-11.61
Nb-SAC	-11.72	-5.90	-8.49
Mo-SAC	-9.99	-4.33	-6.29
Ru-SAC	-9.33	-5.91	-6.82
Rh-SAC	-8.03	-6.64	-5.60
Pd-SAC	-5.75	-4.65	-3.95
Ag-SAC	-3.84	-1.90	-3.66
Cd-SAC	-3.76	-1.49	-2.35
Hf-SAC	-13.84	-6.86	-11.64
Ta-SAC	-13.03	-6.07	-10.75
W-SAC	-12.85	-5.55	-9.62
Re-SAC	-9.45	-4.58	-6.54
Os-SAC	-11.17	-6.23	-7.10
Ir-SAC	-9.79	-7.36	-7.61
Pt-SAC	-7.77	-6.16	-6.66
Au-SAC	-4.70	-4.12	-4.64

Table S2. Thermodynamic stabilities (E_{stab}) of (TM)SAs embedded at Ga single vacancy (Ga-SV), Nitrogen single vacancy (N-SV), and gallium-nitrogen double vacancy (Ga/N-DV) sites. The more negative E_{stab} values indicate the strong metal-support interaction and better stability against metal clustering or being leached.

Catalysts	E_{stab} (eV)		
	Ga-SV	N-SV	Ga/N-DV
Sc-SAC	-8.65	-1.94	-5.50
Ti-SAC	-5.86	-0.24	-3.96
V-SAC	-5.21	1.04	-2.13
Cr-SAC	-2.89	2.00	-1.43
Mn-SAC	-2.16	2.23	-1.54
Fe-SAC	-3.26	1.14	-1.68
Co-SAC	-2.92	0.71	-1.20
Ni-SAC	-2.77	0.33	-1.03
Cu-SAC	-2.57	0.85	-1.38
Zn-SAC	-3.08	-0.31	-3.04
Y-SAC	-9.01	-2.98	-6.09
Zr-SAC	-6.65	-0.53	-4.74
Nb-SAC	-3.95	1.86	-0.73
Mo-SAC	-2.96	2.71	0.75
Ru-SAC	-2.31	1.14	0.21
Rh-SAC	-2.23	-0.84	0.20
Pd-SAC	-2.38	-1.29	-0.58
Ag-SAC	-1.41	0.53	-1.23
Cd-SAC	-3.06	-0.79	-1.65
Hf-SAC	-6.88	0.10	-4.68
Ta-SAC	-4.43	2.53	-2.15
W-SAC	-3.62	3.68	-0.39
Re-SAC	-1.40	3.47	1.51
Os-SAC	-2.55	2.39	1.52
Ir-SAC	-2.69	-0.26	-0.51
Pt-SAC	-2.47	-0.87	-1.36
Au-SAC	-1.88	-1.30	-1.83

Table S3. Electrochemical stabilities (U_{diss}) of (TM)SAs embedded at Ga single vacancy (Ga-SV), Nitrogen single vacancy (N-SV), and gallium-nitrogen double vacancy (Ga/N-DV) sites. U^{o}_{diss} and eN represents the standard dissolution potential of bulk TMs and the number of transferred electrons during the dissolution process, respectively.

Catalysts	U^{o}_{diss} (V)	N_e	U_{diss} (V)		
			Ga-SV	N-SV	Ga/N-DV
Sc-SAC	-2.08	3	0.80	-1.43	-0.25
Ti-SAC	-1.63	2	1.30	-1.51	0.35
V-SAC	-1.18	2	1.43	-1.70	-0.11
Cr-SAC	-0.91	2	0.54	-1.91	-0.19
Mn-SAC	-1.19	2	-0.11	-2.31	-0.42
Fe-SAC	-0.45	2	1.18	-1.02	0.39
Co-SAC	-0.28	2	1.18	-0.64	0.32
Ni-SAC	-0.26	2	1.12	-0.43	0.25
Cu-SAC	0.34	2	1.62	-0.09	1.03
Zn-SAC	-0.76	2	0.78	-0.61	0.76
Y-SAC	-2.37	3	0.63	-1.38	-0.34
Zr-SAC	-1.45	4	0.21	-1.32	-0.26
Nb-SAC	-1.10	3	0.22	-1.72	-0.86
Mo-SAC	-0.20	3	0.79	-1.10	-0.45
Ru-SAC	0.46	2	1.62	-0.10	0.36
Rh-SAC	0.60	2	1.71	1.02	0.50
Pd-SAC	0.95	2	2.14	1.59	1.24
Ag-SAC	0.80	1	2.21	0.27	2.03
Cd-SAC	-0.40	2	1.13	-0.01	0.42
Hf-SAC	-1.55	4	0.17	-1.58	-0.38
Ta-SAC	-0.60	3	0.88	-1.44	0.12
W-SAC	0.10	3	1.31	-1.13	0.23
Re-SAC	0.30	3	0.77	-0.86	-0.20
Os-SAC	0.84	8	1.16	0.54	0.65
Ir-SAC	1.16	3	2.06	1.25	1.33
Pt-SAC	1.18	2	2.42	1.61	1.86
Au-SAC	1.50	3	2.13	1.93	2.11

Table S4. Geometrical parameters of CO_2 molecule after adsorption over various single atom catalysts (SACs). Adsorption energy of CO_2 ($E_{\mathrm{ads}[*\mathrm{CO_2}]}$), angle between O=C=O ($\varphi_{OCO}$), distance from transition metal to carbon atom of adsorbed CO_2 ($d^{TM\text{-}C}$), distance between oxygen and carbon atoms ($d^{O\text{-}C}$), and the corresponding configurations of $CO_2^{\bullet-}$ species.

Catalysts	$E_{\mathrm{ads}[*\mathrm{CO_2}]}$ (eV)	φ_{OCO} (deg.)	$d^{TM\text{-}C}$ (Å)	$d^{O\text{-}C}$ (Å)		$CO_2^{\bullet-}$ Configuration
				1O-C	2O-C	
Sc-SAC	-0.28	179.8	4.55	1.18	1.18	-
Ti-SAC	-1.64	135.8	2.50	1.28	1.22	C_s
V-SAC	-1.39	130.5	2.03	1.31	1.24	C_s
Cr-SAC	-0.41	133.6	1.97	1.30	1.23	C_s
Mn-SAC	-1.10	133.8	2.07	1.26	1.25	C_{2v}
Fe-SAC	-1.08	179.7	4.00	1.18	1.18	-
Co-SAC	-0.97	179.5	3.55	1.18	1.18	-
Ni-SAC	-0.24	179.7	3.50	1.18	1.18	-
Cu-SAC	-0.25	179.7	3.70	1.18	1.18	-
Zn-SAC	-1.22	179.6	3.82	1.18	1.18	-
Y-SAC	-0.27	179.8	4.78	1.18	1.18	-
Zr-SAC	-1.41	135.2	2.43	1.26	1.23	C_{2v}
Nb-SAC	-2.92	126.7	2.17	1.33	1.24	C_s
Mo-SAC	-1.82	129.7	2.08	1.33	1.25	C_s
Ru-SAC	-1.13	125.1	2.04	1.32	1.25	C_{2v}
Rh-SAC	-0.62	129.5	2.04	1.29	1.24	C_{2v}
Pd-SAC	-0.29	179.8	3.89	1.18	1.18	-
Ag-SAC	-0.21	178.3	3.89	1.18	1.18	-
Cd-SAC	-0.33	179.6	4.61	1.18	1.18	-
Hf-SAC	-1.44	133.9	2.32	1.27	1.23	C_{2v}
Ta-SAC	-3.02	125.6	2.17	1.34	1.24	C_s
W-SAC	-1.36	127.7	2.07	1.34	1.25	C_s
Re-SAC	-2.74	125.6	2.10	1.34	1.25	C_{2v}
Os-SAC	-0.61	131.2	2.09	1.27	1.25	C_{2v}
Ir-SAC	-0.30	134.4	2.03	1.26	1.24	C_{2v}
Pt-SAC	0.36	139.7	2.13	1.24	1.23	C_{2v}
Au-SAC	0.02	178.9	3.79	1.18	1.18	-

Table S5. Bader charge analysis of CO_2 adsorbed systems. TM denotes the transition metal, and the CO_2 adsorbate atoms are represented by C, 1O and 2O. The net charge transfer from surface to adsorbed CO_2 is also provided.

Catalysts	TM	C	1O	2O	Net charge on CO_2
Sc-SAC	2.089	2.164	-1.092	-1.095	-0.023
Ti-SAC	1.991	1.507	-1.147	-1.149	-0.789
V-SAC	1.873	1.275	-1.129	-1.224	-1.078
Cr-SAC	1.647	1.380	-1.107	-1.204	-0.930
Mn-SAC	1.437	1.491	-1.202	-1.199	-0.911
Fe-SAC	1.341	2.156	-1.091	-1.084	-0.019
Co-SAC	1.039	2.142	-1.086	-1.090	-0.034
Ni-SAC	0.944	2.151	-1.083	-1.099	-0.031
Cu-SAC	0.884	2.149	-1.086	-1.094	-0.030
Zn-SAC	1.063	2.151	-1.084	-1.090	-0.024
Y-SAC	2.312	2.164	-1.097	-1.092	-0.025
Zr-SAC	2.630	1.524	-1.154	-1.168	-0.794
Nb-SAC	2.266	1.180	-1.178	-1.249	-1.247
Mo-SAC	1.961	1.242	-1.113	-1.236	-1.107
Ru-SAC	1.255	1.411	-1.202	-1.162	-0.953
Rh-SAC	0.075	1.510	-1.154	-1.184	-0.828
Pd-SAC	1.555	2.167	-1.073	-1.071	0.023
Ag-SAC	0.751	2.153	-1.042	-1.047	0.064
Cd-SAC	1.017	2.196	-1.108	-1.102	-0.015
Hf-SAC	2.545	1.531	-1.199	-1.149	-0.817
Ta-SAC	2.410	1.116	-1.162	-1.257	-1.304
W-SAC	2.180	1.132	-1.106	-1.245	-1.218
Re-SAC	1.713	1.282	-1.220	-1.167	-1.105
Os-SAC	2.778	1.371	-1.230	-1.211	-1.070
Ir-SAC	1.058	1.543	-1.140	-1.201	-0.798
Pt-SAC	0.742	1.721	-1.139	-1.164	-0.583
Au-SAC	1.515	2.174	-1.10	-1.103	-0.029

Table S6. DFT calculated electronic energies, zero-point energies, and entropy contributions for the gaseous molecules at T = 298 K.

Species	E_{elec} (eV)	ZPE (eV)	-TS (eV)
CO_2	-22.24	0.31	-0.64
CO	-14.42	0.14	-0.61
HCOOH	-29.22	0.90	-1.03
CH_3OH	-29.93	1.35	-0.78
CH_4	-24.04	1.19	-0.60
H_2O	-14.15	0.57	-0.64
$0.5\times H_2$	-3.495	0.14	-0.20

Table S7. Zero-point energies and entropy contributions to the adsorbate free energy at T = 298 K.

Adsorbate	ZPE (eV)	-TS (eV)
*COOH	0.56	-0.17
*OCHO	0.56	-0.14
*CO	0.20	-0.15
*HCOOH	0.91	-0.19
*CHO	0.46	-0.15
*CHOH	0.81	-0.11
$*CH_2OH$	1.10	-0.16
$*CH_3O$	1.08	-0.16
*O	0.20	-0.16
*OH	0.35	-0.09
*C	0.09	-0.04
*CH	0.32	-0.09
$*CH_2$	0.61	-0.10
$*CH_3$	0.95	-0.12

Table S8. Several CO_2RR products with reaction mechanisms and corresponding equilibrium potentials.

Cathode Reaction	Product	U_{eq} vs RHE (V)
$CO_2 + 2H^+ + 2e^- \rightarrow CO(g) + H_2O$	Carbon monoxide	-0.11
$CO_2 + 2H^+ + 2e^- \rightarrow HCOOH(l) + H_2O$	Formic acid	-0.25
$CO_2 + 6H^+ + 6e^- \rightarrow CH_3OH(l) + H_2O$	Methanol	0.02
$CO_2 + 8H^+ + 8e^- \rightarrow CH_4(g) + 2H_2O$	Methane	0.17

Table S9. Adsorption Gibb's free energies (ΔG) of first protonation step (*COOH or *OCHO) for chemisorbed systems.

Catalysts	ΔG_{*COOH*}	ΔG_{*OCHO}
Ti-SAC	-0.10	-1.44
V-SAC	0.49	-0.61
Cr-SAC	-0.02	-0.74
Mn-SAC	0.29	-0.10
Zr-SAC	0.51	-1.14
Nb-SAC	1.03	0.07
Mo-SAC	0.89	0.18
Ru-SAC	0.66	0.64
Rh-SAC	0.46	0.40
Hf-SAC	0.42	-1.19
Ta-SAC	1.10	0.15
W-SAC	0.44	-0.02
Re-SAC	0.66	0.60
Os-SAC	0.63	1.27
Ir-SAC	0.45	0.62

Table S10. Adsorption Gibbs free energies of elementary reaction steps of CO_2RR over Os and Ir-SAC.

Elementary reaction step	ΔG (eV)	
	Os-SAC	Ir-SAC
$*CO_2^{\bullet-} + H^+ \rightarrow *COOH$	0.63	0.45
$*CO_2^{\bullet-} + H^+ \rightarrow *OCHO$	1.27	0.62
$*COOH + H^+ + e^- \rightarrow *CO + H_2O$	-0.34	-0.29
$*CO + H^+ + e^- \rightarrow *COH$	1.26	1.46
$*CO + H^+ + e^- \rightarrow *CHO$	0.31	0.19
$*COH + H^+ + e^- \rightarrow *C + H_2O$	0.19	0.07
$*COH + H^+ + e^- \rightarrow *CHOH$	-0.11	-0.80
$*C + H^+ + e^- \rightarrow *CH$	-0.32	-0.44
$*CHOH + H^+ + e^- \rightarrow *CH + H_2O$	-0.02	0.42
$*CHO + H^+ + e^- \rightarrow *OCH_2$	1.15	0.54
$*CHO + H^+ + e^- \rightarrow *CHOH$	0.85	0.48
$*OCH_2 + H^+ + e^- \rightarrow *CH_2OH$	-0.41	-0.05
$*OCH_2 + H^+ + e^- \rightarrow *OCH_3$	-0.64	0.14
$*OCH_3 + H^+ + e^- \rightarrow *CH_3OH$	0.19	-0.69
$*OCH_3 + H^+ + e^- \rightarrow *O + CH_4$	-1.82	-1.80
$*CH_2OH + H^+ + e^- \rightarrow *CH_2 + H_2O$	-0.52	-0.63
$*CH_2OH + H^+ + e^- \rightarrow *CH_3OH$	-0.14	-0.61
$*CH + H^+ + e^- \rightarrow *CH_2$	-0.62	-1.05
$*CH_2 + H^+ + e^- \rightarrow *CH_3$	-0.41	-0.21
$*CH_3 + H^+ + e^- \rightarrow *CH_4$	-0.55	-0.60
$*CH_3OH \rightarrow CH_3OH + *$	-0.90	-0.24
$*CH_4 \rightarrow CH_4 + *$	-0.81	-0.65

Table S11. Potential limiting step (PLS), final product, CO_2RR limiting potential ($U_{L(CO_2RR)}$) and corresponding overpotential (η) values are provided for considered TM-SACs.

Catalysts	PLS	Product	$U_{L(CO_2RR)}$ (V)	η (V)
Ti-SAC	*OCHO + H^+ + e^- → *HCOOH	HCOOH	-1.72	1.47
V-SAC	*OCHO + H^+ + e^- → *HCOOH	HCOOH	-1.80	1.55
Cr-SAC	*OCHO + H^+ + e^- → *HCOOH	HCOOH	-1.42	1.17
Mn-SAC	*OCHO + H^+ + e^- → *HCOOH	HCOOH	-0.50	0.25
Zr-SAC	*OCHO + H^+ + e^- → *HCOOH	HCOOH	-1.56	1.31
Nb-SAC	*OCHO + H^+ + e^- → *HCOOH	HCOOH	-1.61	1.36
Mo-SAC	*OCHO + H^+ + e^- → *HCOOH	HCOOH	-1.62	1.37
Ru-SAC	*OCHO + H^+ + e^- → *HCOOH	HCOOH	-1.08	0.83
Rh-SAC	*OCHO + H^+ + e^- → *HCOOH	HCOOH	-0.42	0.17
Hf-SAC	*OCHO + H^+ + e^- → *HCOOH	HCOOH	-1.68	1.43
Ta-SAC	*OCHO + H^+ + e^- → *HCOOH	HCOOH	-1.62	1.37
W-SAC	*OCHO + H^+ + e^- → *HCOOH	HCOOH	-2.17	1.92
Re-SAC	*OCHO + H^+ + e^- → *HCOOH	HCOOH	-2.05	1.80
Os-SAC	*CHO + H^+ + e^- → *CHOH	CH_4	-0.85	1.02
Ir-SAC	*CHO + H^+ + e^- → *CHOH	CH_4	-0.48	0.65